Distal Gene Expression Governed by Lamins and Nesprins via Chromatin Conformation Change

Haihui Zhang[1, 2], Zhengyang Lei[1], Fatemeh Momen-Heravi[2,*], Peiwu Qin[1,*]

[1] Institute of Biopharmaceutical and Health Engineering, Shenzhen International Graduate School, Tsinghua University, Shenzhen, Guangdong, China.
2 Department of Orofacial Sciences, University of California San Francisco, San Francisco, CA, USA

[*]Correspondence should be addressed to Fatemeh Momen-Heravi (fatemeh.momenheravi@ucsf.edu) or Peiwu Qin (pwqin@sz.tsinghua.edu.cn).

Abstract

The nuclear lamina is a vital structural component of eukaryotic cells, playing a pivotal role in both physiological processes, such as cell differentiation, and pathological conditions, including laminopathies and cancer metastasis. Lamina associated proteins, particularly lamins and nesprins, are integral to mechanosensing, chromatin organization, and gene regulation. However, their precise contributions to gene regulation remain incompletely understood. This study explores the functions of lamin A, LMNA, and SYNE2 in gene expression, with a particular focus on their influence on distal chromatin interactions and conformational changes. Using inducible shRNA knockdown, RNA-seq analysis, and dCas9-mediated live imaging of chromosomes, we demonstrate that lamin A affects RNA synthesis, LMNA governs chromatin spatial organization, and SYNE2 regulates chromatin modifications. Furthermore, both lamins and nesprins enhance telomere dynamics. These findings elucidate nuclear envelope-associated mechanisms in gene regulation, offering valuable insights into chromatin dynamics under both physiological and pathological contexts.

Keywords: RNA-seq, Lamin A, LMNA, Nesprin, SYNE2, dCas9, telomere live-cell imaging

1. Introduction

The three-dimensional organization of the genome within the nucleus plays a crucial role in coordinating gene expression, ensuring the stable repression of heterochromatin while permitting the dynamic regulation of transcriptionally active regions. This organization is intimately connected to the nuclear envelope, a specialized membrane enriched with proteins that actively contribute to chromatin architecture and gene regulation[1]. Among these proteins, the nuclear lamina- a filamentous meshwork of intermediate filament (IF) proteins known as lamins—forms a structural scaffold that anchors chromatin to the nuclear periphery, thereby influencing nuclear mechanics and genomic stability [2]. Lamins interact with the linker of nucleoskeleton and cytoskeleton (LINC) complex to form a direct mechanotransduction bridge that links the cytoskeleton to the extracellular matrix (ECM) while simultaneously influencing chromatin topology. A-type lamins, encoded by the *LMNA* gene, include lamin A and lamin C, whereas B-type lamins (*LMNB1* and *LMNB2*) maintain constitutive roles in nuclear structure across different cell types[3–7].

Lamins have been implicated in diverse biological processes, including stem cell differentiation, cancer progression, aging, and laminopathies, underscoring their multifaceted role in nuclear integrity and genome regulation. Nesprins, giant spectrin-repeat proteins of the LINC complex, serve as critical linkers between the

cytoskeletal filaments and the nuclear lamina, providing structural integrity and modulating intracellular signaling [8,9].

While significant progress has been made in understanding the role of lamins in genome organization, the precise mechanisms by which lamins and nesprins regulate gene expression through distal chromatin interactions remain incompletely understood. Notably, recent evidence suggests a reciprocal interplay between transcription and chromatin conformation, where gene activity can influence chromatin folding and vice versa[10]. However, whether lamins and nesprins actively govern chromatin remodeling and isoform switching beyond their well-characterized functions in mechanotransduction remains an open question.

Lamina-associated domains (LADs) represent large chromatin regions tethered to the nuclear lamina and are generally transcriptionally repressive, enriched with heterochromatic marks such as H3K9me2/3 and H3K27me3. These domains play a pivotal role in nuclear architecture by segregating active and inactive chromatin compartments. Disruptions in LAD organization have been implicated in diseases such as cancer and laminopathies, highlighting the importance of nuclear envelope components in maintaining genomic stability. However, the extent to which lamins and nesprins regulate distal non-LAD chromatin interactions and isoform switching remain largely unexplored.[11,12]

This study aims to dissect the roles of lamin A, LMNA, and SYNE2 in gene expression and chromatin organization, focusing on their influence on distal

chromatin interactions and isoform switching. Using inducible shRNA-mediated knockdown, RNA sequencing (RNA-seq), and dCas9-based live-cell imaging of chromosomes, we systematically investigate their contributions to chromatin conformation and transcriptional regulation. Our findings reveal that lamin A is essential for RNA synthesis, LMNA orchestrates chromatin spatial organization, and SYNE2 modulates chromatin modifications. Furthermore, we demonstrate that both lamins and nesprins impact telomere dynamics, linking nuclear envelope function to chromatin behavior.

By uncovering distinct, isoform-specific and spatially segregated transcriptional responses, our study provides new mechanistic insights into how nuclear lamina components regulate distal gene expression. These findings have broad implications for understanding nuclear architecture in both physiological and pathological contexts, including cancer, aging, and laminopathies.

2. Materials and methods

2.1 Cell culture

Human osteosarcoma (U2OS) cells (#HTB-96, ATCC, USA) and human embryonic kidney (HEK293T) cells (#CRL-3216, ATCC, USA) were cultured in modified Dulbecco's Modified Eagle's Medium (#11965092, DMEM; Gibco), supplemented with 10% fetal bovine serum (FBS). U2OS cells were cultured using HyClone™ characterized tetracycline-screened FBS (#SH30071.03T) at a density of 5×10^4 cells

per cm^2 for RNA extraction experiments, and at a density of 1×10^3 cells per cm^2 for Chromosomes live imaging experiments. While HEK293T cells were cultured with Gibco FBS (#A5256701) at an intial density of 5×10^4 cells per cm^2. The medium also contained 100 U ml^{-1} penicillin and 100 µg ml^{-1} streptomycin (#15140122, Gibco). All cultures were maintained in a humidified incubator at 37 °C with 5% CO_2.

2.2 Construction of stable U2OS cells within inducible shRNA plasmids

To generate the doxycycline-inducible knockdown stable cell lines of Scramble, Lamin A, LMNA, SYNE2 shRNAs. targeting shRNAs (**Supplementary Table S1**) were cloned into the pLKO-Tet-On (#21915, Addgene) inducible vectors by AgeI and EcoRI restriction enzymes (New England Biolabs, USA). HEK293T cells were transfected with pLKO-Tet-On-shRNA, pPAX2 and pMD2 with ratio of 1:1 using Lipofectamine™ 3000 (#L3000015, ThermoFisher Scientific, USA). Lentiviral supernatants were harvested after 48 h, filtered through a 0.45-µm filter, and stored at −80 °C until further use. The Multiplicity of Infection (MOI) was determined by limiting dilution of lentiviral particles. U2OS cells were infected with lentivirus at an MOI of 0.8 in the presence of 8 µg ml^{-1} polybrene (#H9268, Hexadimethrine bromide; MilliporeSigma, USA). Following infection, cells were selected for five days using 4 µg ml^{-1} puromycin (#P4512, MilliporeSigma, USA). Single-cell clones were subsequently isolated and expanded in the presence of 2 µg ml^{-1} puromycin to establish doxycycline-inducible shRNA-knockdown stable cell lines. For

doxycycline-inducible shRNA-knockdown stable cell lines, the cells were treated with 100 ng ml^{-1} doxycycline (#D5207, MiliporeSigma, USA) for 48 hours.

2.3 Reverse transcription quantitative real-time PCR (RT-qPCR)

The knockdown efficiency of targeting genes in the stable U2OS cells containing inducible shRNA plasmids was assessed using RT-qPCR. Total RNA was extracted by Trizol (#T3934, MiliporeSigma, USA), 500 ng of total RNA was used as a template for reverse transcription into cDNA using the High-Capacity cDNA Reverse Transcription Kit (#4374966, ThermoFisher Scientific, USA) and real-time PCR was performed using PowerUp™ SYBR™ Green Master Mix (#A25778, ThermoFisher Scientific, USA). For the procedure of real-time PCR, cDNA templates, SYBR, and primers were mixed and loaded to Applied Biosystems™ 7500 Real-Time PCR Systems, started with an initial denaturation at 95 °C for 300 seconds to separate DNA strands. Following 40 cycles of denaturation (95 °C for 20 seconds), annealing (55 °C for 20 seconds), and extension (72 °C for 20 seconds). The relative transcript abundance was initially normalized to GAPDH and subsequently adjusted relative to the no-doxycycline-treated controls using the ΔΔCt method. Primer sequences are shown in **Supplementary Table S2**.

2.4 Library preparation for transcriptome sequencing (RNA-seq)

Total RNA, including mRNA and lncRNA, was used to prepare sequencing libraries.. RNA was purified from total RNA using probes to remove rRNA by Ribo-Zero rRNA Removal Kit (#15066012, Illumina, USA). RNA integrity and quantification were

assessed using the Bioanalyzer 2100 system (Agilent Technologies, USA). RNA was fragmented with divalent cations at high temperature in a First Strand Synthesis Reaction Buffer (5×). First strand cDNA was synthesized with random hexamer primers and M-MuLV Reverse Transcriptase (RNase H), followed by second strand cDNA Synthesis using DNA Polymerase I and RNase H. The concentration of cDNAs in the library was quantified to 1 ng μl^{-1} using a Qubit 2.0 fluorometer. Overhangs were converted to blunt ends using exonuclease and polymerase activities. After adding adenylated 3' ends to the DNA fragments, NEBNext Adapters with hairpin loops were ligated for hybridization.

To select cDNA fragments 370–420 bp in length, libraries were purified with the AMPure XP system (Beckman Coulter). Size-selected, adaptor-ligated cDNA was treated with 3 µl USER Enzyme (New England Biolabs) at 37 °C for 15 minutes, followed by 95 °C for 5 minutes. PCR amplification was performed using Phusion High-Fidelity DNA Polymerase, Universal PCR primers, and Index (X) primers. The PCR products were purified using the AMPure XP system, and library quality was assessed using the Agilent Fragment Analyzer 5400 system.

Clustering of index-coded samples was carried out on a cBot Cluster Generation System using the TruSeq PE Cluster Kit v3-cBot-HS (Illumina) according to the manufacturer's protocol. Finally, libraries were sequenced on an Illumina Novaseq 6000 platform, generating 150 bp paired-end reads.

2.5 Telomere tracking in live cells by dCas9 imaging

The *S. pyogenes* Cas9 gene, modified with D10A and H840A mutations (dCas9), was engineered to include a 2× SV40 nuclear localization sequence (NLS) and a 3× Flag-tag at the N-terminus, as well as GFP at the C-terminus [13,14]. These dCas9 constructs were cloned into a lentiviral vector driven by the SFFV promoter. To establish a stable dCas9-expressing cell line, cells were transduced with the lentivirus, selected with 5 μg ml^{-1} puromycin for five days, and subsequently sorted via fluorescence-activated cell sorting (FACS) [14,15]. The sgRNA plasmids were expressed under the U6 promoter, with the original plasmid backbone modified to include TagBFP as a transduction marker. The sgRNA sequences were amplified from an oligo template containing the 20-nucleotide telomere-targeting sequence: GUUAGGGUUAGGGUUAGGGUUA. For viral transduction, cells were incubated with a virus solution diluted threefold in DMEM medium supplemented with 10 μg ml^{-1} polybrene for 24 hours. For imaging telomere dynamics, fluorescence signals were captured using TIRF microscopy on a Nikon ECLIPSE Ti2 inverted microscope equipped with a Hamamatsu C11440-22C digital CMOS camera. The imaging parameters included an 80° incident angle, 200 ms intervals, and 300 ms exposure time. The laser power was set to 0.8 mW, and the gamma parameter was adjusted to 1[16,17]. At least 20 individual cells were examined for each case in the analysis. Telomere movement was tracked using CellProfiler software (version 4.2.25, https://cellprofiler.org/).

2.6 RNA-seq analysis

For trimming, trimming procedure was first applied to eliminate adapter sequences present in our data and to improve read quality from the FASTQ files. Adapter removal and quality trimming were carried out using Trimmomatic (v0.35). In all cases only reads with a Phred quality score > 20 and read length > 50 bp were selected for downstream analysis. Paired-end reads were removed if either read contained more than 10% ambiguous bases (N). Additionally, reads were discarded if more than 50% of their bases had a quality score of ≤ 5. Reads containing adapter sequences were also excluded from further analysis. Each sample produced approximately 80 million sequencing reads after quality control. We then use Salmon (v1.8.0) pseudoalignment to perform alignment, counting and normalization in one single step. The isoform switching was analyzed using the IsoformSwitchAnalyzeR (v1.14.1) [18]. The isoform switches were identified and quantified from RNA-seq data by using gtf annotaion files from gencode (v47). IsoformSwitchAnalyzeR assesses isoform usage by calculating isoform fraction (IF) values, which represent the proportion of a gene's total expression attributed to a specific isoform. This is determined by dividing the expression level of the isoform by the overall gene expression. Changes in isoform usage are quantified as the difference in isoform fraction (dIF), computed as IF2 − IF1. These dIF values are subsequently utilized to determine the isoform log2 fold change.

2.7 Statistical analysis

Each experiment was performed with a minimum of three replicates. All the analysis and comparisons were performed in R (v4.2.0). The DESeq2 (v1.46.0) package was

utilized to analyze the differences between the doxycycline-treated groups and the untreated groups [19]. Differential gene analysis was performed with a baseMean threshold of > 50 and a significance level of *p*-value < 0.05. Benjamini-Hochberg (BH) procedure was employed to control the false discovery rate (FDR) in multiple hypothesis testing (*q*-value). The resulting differential expressed gene (DEG) lists, ranked in descending order, were subsequently employed for Gene Ontology (GO) enrichment analysis using the clusterProfiler package (v3.20) [20]. For significant levels of multiple group comparison, non-parametric Kruskal-Wallis test was used to compare the medians of multiple groups.

3. Results

3.1 Efficient knockdown of lamins and nesprins

Linker of nucleoskeleton and cytoskeleton (LINC) complex component nesprin-2 locates in the nuclear envelope to link the actin cytoskeleton and the nuclear lamina, which maitains cellular structure and serves as mechanotransducers between nuclear and extracellular matrix (ECM) [8]. lamin proteins weave a filamentous network in the inner nuclear interior to form lamina meshwork, which provides chromosomal anchoring sites to maintain genome organization. nucleoplasmic lamins bind to chromatin and have been indicated to regulate chromatin accessibility and spatial chromatin organization [21]. However, the contribution of nesprins and lamins to gene expression has not been fully understood.

Herein, we performed an extensive study of how nesprins and lamins regulate gene expression by performing RNA-seq and RT-qPCR when knockdown of nesprins and lamins by inducible shRNA expression. Our results demonstrated that Lamin A could affect RNA synthesis. LMNA could influence chromatin conformation change. SYNE2 (nesprin-2) could modulate chromatin modification (**Figure 1a**). In this work, shScramble, shLaminA, shLMNA, and shSYNE2 were denoted as comparisons between doxycycline-treated groups and untreated groups. Herein, shScramble groups were used to rule out non-specific effects. Doxycycline inducible shRNA expressing cells with scramble shRNA were chosen as control to exclude non-specific targeting effect. A fragment of shRNA that targeting 3' untranslated region (UTR) region in LMNA genes was chosen to knockdown lamin A (shLaminA). A fragment of shRNA that targeting coding sequence (CDS) region in LMNA genes was chosen to knockdown LMNA (shLMNA). A fragment of shRNA that targeting coding sequence (CDS) region in SYNE2 genes was chosen to knockdown nesprin-2 (shSYNE2). The targeting shRNA sequences were listed in **Supplementary Table S1**.

The relative gene expression and log2 fold change were quantified in doxycycline-treated groups versus untreated groups for RT-qPCR and RNA-seq data, respectively. For RT-qPCR analysis in shScramble comparisons, the mean ± s.d. relative gene expression ratio was 0.96 ± 0.15 for lamin A, 0.95 ± 0.15 for LMNA, 1.03 ± 0.16 for SYNE2; For RNA-seq analysis in shScramble comparisons, the mean log2 fold change was 0.14 ± 0.10 for lamin A, 0.06 ± 0.05 for LMNA, 0.04 ± 0.11 for

SYNE2. These data indicated that scramble shRNA did not change gene expression to the target genes. In contrast, targeting shRNAs significantly reduced the corresponding target genes. For RT-qPCR analysis, the mean ± s.d. relative gene expression ratio was 0.33 ± 0.01 for lamin A in shLaminA comparisons, 0.30 ± 0.02 for LMNA in shLMNA comparisons, 0.21 ± 0.04 for SYNE2 in shSYNE2 comparisons; For RNA-seq analysis, the mean log2 fold change was −1.34 ± 0.08 for lamin A in shLaminA comparisons, 0.64 ± 0.06 for LMNA in shLMNA comparisons, −0.87 ± 0.22 for SYNE2 in shSYNE2 comparisons (**Figure 1b**). Herein, we employed IsoformSwitchAnalyzeR to quantify log2 fold change of lamin A isoform (**Supplementary Figure S1**). Our findings demonstrated a significant reduction in the utilization of the lamin A isoform, while the expression levels of other LMNA gene isoforms remained unchanged. Together, our results indicated the efficient knockdown of lamin A, LMNA and SYNE2 genes. Knockdown of lamin A specifically reduced the usage of its primary isoform, suggesting a potential role in chromatin architecture regulation, while other LMNA isoforms remained unaffected, highlighting a selective effect. Together, our results indicated the efficient knockdown of lamin A, LMNA, and SYNE2 genes.

3.2 Impact of lamins and nesprins on RNA biosynthesis, chromatin conformation, and modification

Correlation heatmap and principal component analysis (PCA) plot revealed distinct gene expression profiles across the shScramble, shLaminA, shLMNA, and shSYNE2

groups (**Supplementary Figure S2**). Next, by performing DE analysis with DESeq2, our data showed that depletion of lamins and nesprins could significantly lead to the alternation of gene expression, inlcuding the protein-coding mRNAs and long non-coding lncRNAs (**Supplementary Table S3**). To examine pathway enrichment by the DEGs in the shLaminA, shLMNA, and shSYNE2 comparisons. GO analysis on biological process (BP) was conducted by clusterProfiler package, which was based on the hypergeometric test of desending ranking of log2 fold change of DEGs. No significant BP pathway was enriched for shScramble comparison (**Supplementary Figure S3**). Intriguingly, RNA synthesis pathways were enriched in the knockdown of lamin A isoform, including purine-containing compound metabolic process and ribose phosphate metabolic process, which ensure the synthesis of the ribonucleotide triphosphates (NTPs) that required for RNA synthesis (**Figure 2a**). In contrast, the knockdown of the LMNA gene was associated with an enrichment of DNA conformation change, suggesting that LMNA may regulate alterations in the spatial organization of chromatin (**Figure 2b**). In addition, the knockdown of the SYNE2 gene was linked to ncRNA metabolic process and covalent chromatin modification, indicating that the impact of SYNE2 in the regulation of chromatin accessibility, remodeling and gene expression (**Figure 2c**).

3.3 Role of lamins and nesprins in isoform switches

To investigate how lamins and nesprins would influence isoform swithes, we performed isoform switches analysis by IsoformSwitchAnalyzeR package. By

ascending ranking of *q*-values of isoform switches, the top 10 isoform genes including TARS1, PPP1R13L, ATP6AP2, NBL1, JADE1, AGPS, Lnc-ZFAT-1, RBM11, and PEX19 were significant changed in the knockdown of lamin A gene (**Figure 3a**). These proteins are involved in protein synthesis (TARS1), chromatin remodeling (JADE1), RNA (RBM11), and protein degration (ATP6AP2, PEX19). The top isoform genes including SAFB2, LIN54, DUXAP9, BCAS3, G6PD, TEAD2, AHR, PAM, and ZFHX4 were significant changed in the knockdown of LMNA gene (**Figure 3b**). These proteins are involved in transcriptional repressors (SAFB2, LIN54), transcription factor (TEAD2, AHR, ZFHX4), and post-translational modification (PAM). The top isoform genes including HNRNPK, ILF3, HNRNPA1, DUXAP9, RPS27, LDHB, CALU, SNHG29, HNRNPDL, and EDC3 were significant changed in the knockdown of LMNA gene (**Figure 3c**). These proteins are involved in RNA splicing and stability (HNRNPK, ILF3, HNRNPA1, HNRNPDL), mRNA decay (EDC3), and protein synthesis and folding (RPS27, RPS27).

Nesprin-2 depletion induced a substantially larger number of DE isoforms (n = 4505) compared to lamin A (n = 1326) and *LMNA* (n = 1156) gene knockdown. This included 645 DE long non-coding lncRNAs and 3860 DE mRNAs in nesprin-2 knockdown cells, as well as 273 DE lncRNAs and 1053 DE mRNAs following lamin A silencing, and 263 DE lncRNAs and 893 DE mRNAs after *LMNA* reduction (**Figure 3d**). While the number of DEGs identified for lamins was limited, a significant number of isoform switches was observed following lamin knockdown.

Interestingly, The UpSet plot analysis revealed a high degree of specificity in the gene expression changes induced by each gene knockdown. Minimal overlaps were observed between the differentially expressed genes in shSYNE2, shLaminA, and shLMNA conditions: shSYNE2 and shLaminA (16 lncRNAs, 8 mRNAs), shSYNE2 and shLMNA (12 lncRNAs, 50 mRNAs), and shLaminA and shLMNA (4 lncRNAs, 33 mRNAs), suggesting distinct downstream effects of each gene knockdown. Relative to the shScramble control (median isoform log2 fold change, 1.58), knockdown of LMNA, LaminA, and SYNE2 resulted in substantial changes in isoform expression, with median log2 fold changes of 1.03, 1.23, and −1.33, respectively. Notably, shSYNE2 induced overall reduction of isoform switches. Together, our results demonstrated that Each gene knockdown from lamin A isoform, LMNA an SYNE2 genes induced distinct and highly specific changes in isoform switches.

3.4 Regulation of gene expression in distal non-LAD regions by lamins and nesprins

The majority of genes located within LADs tend to be transcriptionally repressed or expressed at low levels. This is because LADs are associated with heterochromatin , a tightly packed form of DNA that is generally inaccessible to the cellular machinery required for gene expression. Lamin mutations have shown to disrup LAD organization and gene expression that have been implicated in various diseases, including cancer and laminopathies. Next, we investigated the chromosome

localizations of DE mRNAs in the genome-wide. Expectedly, the DEGs from depletion of lamin A, LMNA, and SYNE2 were seldomly intersected with genes in LADs (**Figure 4a**). Consistent with prior studies, depletion of lamin A, LMNA, and SYNE2 did not significantly impact LAD-associated genes, reinforcing the idea that their primary function in gene regulation may occur in distal non-LAD chromatin regions [12].

Interestingly, the DEGs from depletion of lamin A, LMNA, and SYNE2 were dispersed in different chromosome loci when mapping genes to human hg19 genome reference. The DEGs from depletion of lamin A were located in chr8q13, chr10q21, and chr11q25. The DEGs from depletion of LMNA were mainly located in chr20q13, chr3q13, and chr19p12. The DEGs from depletion of SYNE2 were mainly located in chr9q34, chr1p36, and chr17q21 (**Figure 4b**). To confirm that the DEGs were not located in LADs, we measured the spatial distance between LADs and DEGs in shLaminA, shLMNA, and shSYNE2 through GenometriCorr package. Our data suggested that those DEGs are spatially far away from LADs (**Figure 4c**). Together, our results demonstrated that the depletion of lamin A, LMNA, and SYNE2 led to the change of gene expression in distal non-LADs.

3.5 Modulation of lncRNA-mRNA interactions in the nuleus by lamins and nesprins

In accordance to published results, our data also indicated the low expression profiling of lncRNAs compared to mRNA expression profiling (**Supplementary**

Figure S4) [22]. Interestingly, the mRNA expression profiling demonstrated continuously unimodal distribution through density plot of log2 transcript per million (Log2TPM). In contrast, the lncRNA expression profiling demonstrated multimodal dsitribution with multiple peaks (**Figure 5a**). In addition, our predictions showed that lncRNAs are mainly located in nucleus through analysis with DeepLncLoc algorithm (**Figure 5b**) [23]. The results suggested that mRNA-lncRNA interactions were mainly occured in nucleus.

Furthermore, cis-acting mRNA-lncRNA interaction pairs were also obtained by searching highly correlated expression levels between mRNAs and lncRNAs in the10kb windows in the genome-wide (**Figure 5c**). Additionally, the lncTar algorithm and peason correlation test were employed to analyze lncRNA-mRNA coexpression networks, enabling the identification and validation of trans-acting and/or cis-acting lncRNA-mRNA interaction networks [24]. We identified two interaction networks between two lncRNAs (green nodes) and their associated mRNAs (orange nodes). Upregulated genes are represented as triangles, while downregulated genes are shown as circles. Two clusters are centered around the lncRNAs AC009961.3 and SCARNA2, highlighting their regulatory roles in specific gene expression pathways. The networks underscored the potential mechanistic influence of lncRNAs in cellular processes and their functional impact on mRNA expression (**Figure 5d**).

3.6 Increased telomere dynamics with lamins and nesprins depletion

To investigate the role of lamins and nesprins in spatial and temporal organization and dynamic behaviors of chromatin, we utilized enhanced green fluorescent protein (EGFP)-tagged dCas9 to visualize telomeric regions of the genome containing repetitive elements in living U2OS cells, allowing us to analyze telomere movement [15]. Representative fluorescence images of telomeres labeled with EGFP-dCas9 in U2OS cells are shown in **Figure 6a**. Notably, depletion of lamin A, LMNA, and SYNE2 resulted in significantly increased genome dynamics and a larger nuclear area scanned. This effect was quantified through telomere mean square displacement (MSD) analysis and the measurement of traveled distance within a 30-second imaging window (**Figure 6b, c and Supplementary Movie S1**). These findings support the concept that lamins play a critical role in regulating chromatin dynamics [25]. Collectively, our results highlight a regulatory function of lamins and nesprins in controlling chromatin behavior.

4. Discussion

LADs collectively account for approximately 40% of the genome, though not all of these regions are bound to the nuclear lamina across all cells within a population. Defined by their physical interaction with the nuclear lamina, LADs are characterized by low gene density—containing approximately 2–3 genes per megabase, in contrast to the human genome's average of 8 genes per megabase. These regions are enriched

with repressive chromatin features, limiting transcriptional activity compared to non-LAD regions, which are typically more transcriptionally active [11].

Our findings reveal distinct functional roles for Lamin A, LMNA, and SYNE2 in chromatin regulation and gene expression, providing key insights into the spatial organization of the genome. Notably, Lamin A depletion led to enrichment of pathways associated with RNA biosynthesis, supporting its previously suggested role in transcriptional activation and ribonucleotide metabolism. This aligns with prior studies indicating that Lamin A contributes to chromatin accessibility and RNA polymerase activity. In contrast, LMNA knockdown was linked to alterations in chromatin conformation, underscoring its role in maintaining spatial chromatin organization and nuclear stability. Given that LMNA mutations have been implicated in various laminopathies and genome instability disorders, these findings provide a mechanistic framework linking LMNA function to nuclear integrity.

The findings that DEGs are predominantly located in non-LAD regions highlight a unique regulatory aspect of lamins and nesprins, emphasizing their spatial specificity in gene expression. Moreover, the modulation of lncRNA-mRNA interactions by these proteins unveils a layered regulatory network, further illustrating the nuclear envelope's influence on transcriptional dynamics. The isoform switching patterns observed following knockdown of Lamin A and LMNA provide further insight into transcriptomic flexibility. Our data show that Lamin A knockdown specifically reduced the usage of its primary isoform, suggesting a potential role in chromatin

architecture regulation, while other LMNA isoforms remained unaffected, highlighting a selective effect. Given that lamin isoforms are known to differentially impact nuclear stiffness and mechanotransduction, these findings raise the possibility that specific lamin isoforms may be preferentially required for distinct chromatin interactions and nuclear functions.

These results resonate with existing studies linking nuclear envelope dysfunction to diseases such as laminopathies and cancer [4,26,27], where altered nuclear mechanics and chromatin misregulation are hallmarks of disease progression. The observed enhancement of chromatin dynamics upon depletion of Lamin A, LMNA, and SYNE2, as visualized through dCas9-based live chromosome imaging, suggests that these nuclear envelope proteins contribute to chromatin rigidity and nuclear compartmentalization. Their depletion leads to increased chromatin fluidity, which may underlie genomic instability and misregulated transcription in disease states.

By elucidating the molecular mechanisms underlying chromatin behavior, this study contributes to the growing understanding of nuclear architecture as a key regulator of cellular homeostasis. These insights may have broad implications for understanding nuclear envelope-associated diseases, particularly those involving mutations in LMNA or SYNE2, and may help guide future therapeutic strategies targeting nuclear envelope dysfunction.

5. Conclusion

In summary, this study demonstrates the intricate roles of lamin A, LMNA, and SYNE2 in regulating distal chromatin and gene expression. Using inducible knockdown systems and transcriptomic analyses, we identified their distinct contributions to RNA synthesis, chromatin conformation, and modifications. Using dCas9-based live chromosome imaging, enhanced chromatin dynamics were oberserved for the depletion of lamin A, LMNA, and SYNE2 genes. These findings enhance our understanding of nuclear envelope-associated gene regulation and its implications for diseases involving chromatin misregulation. Future research should explore the broader impact of these mechanisms in diverse cellular contexts, advancing potential therapeutic strategies targeting nuclear envelope dysfunction.

6. Data availability

BED file were retrieved from lamin A/C CHIP-seq (https://github.com/kohta-ikegami/pS22-LMNA/blob/master/E1_BJ5ta_LAD.bed)[28]. All the processed data are provided in the Supplementary Tables. All raw sequencing data produced in this study have been deposited in the NCBI SRA database under accession number PRJNA1212085.

Compliance and ethics

The authors declare no conflicts of interest or personal relationships influencing this work.

Acknowledgements

This work is partially supported by the National Natural Science Foundation of China (Grant No. 32350410397); Shenzhen Medical Research Funds (Grant No. D2301002); and the Science, Technology, and Innovation Commission of Shenzhen Municipality (Grant Nos. JCYJ20240813112016022, JCYJ20220530143014032, JCYJ20230807113017035, KCXFZ20211020163813019).

References

1. Buchwalter, A., Kaneshiro, J. M. & Hetzer, M. W. Coaching from the sidelines: the nuclear periphery in genome regulation. *Nat Rev Genet* **20**, 39–50 (2019).
2. Karoutas, A. & Akhtar, A. Functional mechanisms and abnormalities of the nuclear lamina. *Nat Cell Biol* **23**, 116–126 (2021).
3. Irianto, J., Pfeifer, C. R., Ivanovska, I. L., Swift, J. & Discher, D. E. Nuclear Lamins in Cancer. *Cel. Mol. Bioeng.* **9**, 258–267 (2016).
4. Bell, E. S. *et al.* Low lamin A levels enhance confined cell migration and metastatic capacity in breast cancer. *Oncogene* **41**, 4211–4230 (2022).
5. Scaffidi, P., Gordon, L. & Misteli, T. The Cell Nucleus and Aging: Tantalizing Clues and Hopeful Promises. *PLOS Biology* **3**, e395 (2005).
6. Shah, P. P. *et al.* Pathogenic LMNA variants disrupt cardiac lamina-chromatin interactions and de-repress alternative fate genes. *Cell Stem Cell* **28**, 938-954.e9 (2021).
7. Swift, J. *et al.* Nuclear Lamin-A Scales with Tissue Stiffness and Enhances Matrix-Directed Differentiation. *Science* **341**, 1240104 (2013).
8. Rajgor, D. & Shanahan, C. M. Nesprins: from the nuclear envelope and beyond. *Expert Reviews in Molecular Medicine* **15**, e5 (2013).
9. Li Mow Chee, F. *et al.* Mena regulates nesprin-2 to control actin–nuclear lamina associations, trans-nuclear membrane signalling and gene expression. *Nat Commun* **14**, 1602 (2023).

10. van Steensel, B. & Furlong, E. E. M. The role of transcription in shaping the spatial organization of the genome. *Nat Rev Mol Cell Biol* **20**, 327–337 (2019).

11. Briand, N. & Collas, P. Lamina-associated domains: peripheral matters and internal affairs. *Genome Biology* **21**, 85 (2020).

12. Steensel, B. van & Belmont, A. S. Lamina-Associated Domains: Links with Chromosome Architecture, Heterochromatin, and Gene Repression. *Cell* **169**, 780–791 (2017).

13. Bandaria, J. N., Qin, P., Berk, V., Chu, S. & Yildiz, A. Shelterin Protects Chromosome Ends by Compacting Telomeric Chromatin. *Cell* **164**, 735–746 (2016).

14. Qin, P. *et al.* Live cell imaging of low- and non-repetitive chromosome loci using CRISPR-Cas9. *Nat Commun* **8**, 14725 (2017).

15. Chen, B. *et al.* Dynamic Imaging of Genomic Loci in Living Human Cells by an Optimized CRISPR/Cas System. *Cell* **155**, 1479–1491 (2013).

16. Lei, Z. *et al.* Detection of Frog Virus 3 by Integrating RPA-CRISPR/Cas12a-SPM with Deep Learning. *ACS Omega* **8**, 32555–32564 (2023).

17. He, Q. *et al.* Unraveling the influence of CRISPR/Cas13a reaction components on enhancing trans-cleavage activity for ultrasensitive on-chip RNA detection. *Microchim Acta* **191**, 466 (2024).

18. Vitting-Seerup, K. & Sandelin, A. IsoformSwitchAnalyzeR: analysis of changes in genome-wide patterns of alternative splicing and its functional consequences. *Bioinformatics* **35**, 4469–4471 (2019).

19. Love, M. I., Huber, W. & Anders, S. Moderated estimation of fold change and dispersion for RNA-seq data with DESeq2. *Genome Biology* **15**, 550 (2014).

20. Wu, T. *et al.* clusterProfiler 4.0: A universal enrichment tool for interpreting omics data. *The Innovation* **2**, 100141 (2021).

21. Borsos, M. *et al.* Genome–lamina interactions are established de novo in the early mouse embryo. *Nature* **569**, 729–733 (2019).

22. Mattick, J. S. *et al.* Long non-coding RNAs: definitions, functions, challenges and recommendations. *Nat Rev Mol Cell Biol* **24**, 430–447 (2023).

23. Zeng, M. *et al.* DeepLncLoc: a deep learning framework for long non-coding RNA subcellular localization prediction based on subsequence embedding. *Briefings in Bioinformatics* **23**, bbab360 (2022).

24. Li, J. *et al.* LncTar: a tool for predicting the RNA targets of long noncoding RNAs. *Briefings in Bioinformatics* **16**, 806–812 (2015).

25. Bronshtein, I. *et al.* Loss of lamin A function increases chromatin dynamics in the nuclear interior. *Nat Commun* **6**, 8044 (2015).

26. Schreiber, K. H. & Kennedy, B. K. When Lamins Go Bad: Nuclear Structure and Disease. *Cell* **152**, 1365–1375 (2013).

27. Chow, K.-H., Factor, R. E. & Ullman, K. S. The nuclear envelope environment and its cancer connections. *Nat Rev Cancer* **12**, 196–209 (2012).

28. Ikegami, K., Secchia, S., Almakki, O., Lieb, J. D. & Moskowitz, I. P. Phosphorylated Lamin A/C in the Nuclear Interior Binds Active Enhancers Associated with Abnormal Transcription in Progeria. *Developmental Cell* **52**, 699-713.e11 (2020).

Figures and figure legends:

Figure 1

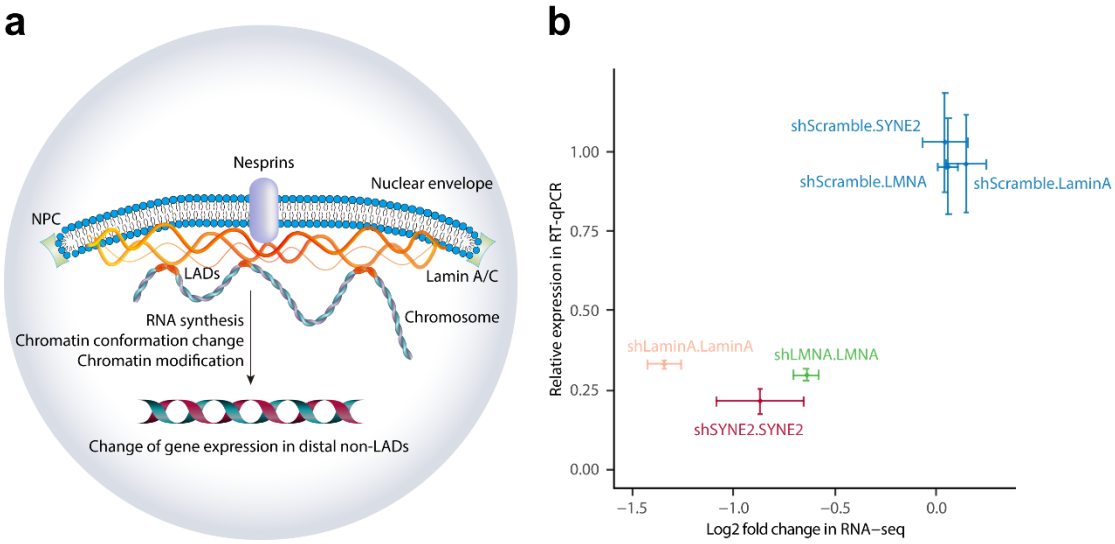

Figure 1. Knockdown of lamins and nesprins alters gene expression. **a)** Schematic illustration of the regulation of gene expression by lamins and nesprins. The lamins and nesprins could affect gene expression in distal non-LADs through altering RNA synthesis, chromatin conformation change, and chromatin modification. NPC, nuclear pore complex; LADs, lamina-associated domains. **b)** Knockdown of lamin A, LMNA, and SYNE2 mRNA levels by targeting shRNAs (shLaminA, yellow; shLMNA, green; shSYNE2, red) was quantified by RT-qPCR and RNA-sequencing (RNA-seq), respectively. In contrast, the relative gene levels of targeting genes (Lamin A, LMNA, SYNE2) are unchanged in the U2OS cells with scramble shRNA construct (shScramble, blue). U2OS cells were treated or untreated with 100 ng ml^{-1} doxycycline for 48 h. The isoform log2 fold change of lamin A was calculated by IsoformSwitchAnalyzeR package. Data represent mean ± s.d. qPCR, n = 7 per group, *p*-value < 0.05; RNA-seq, n = 3 per group, *q*-value < 0.05.

542

Figure 2

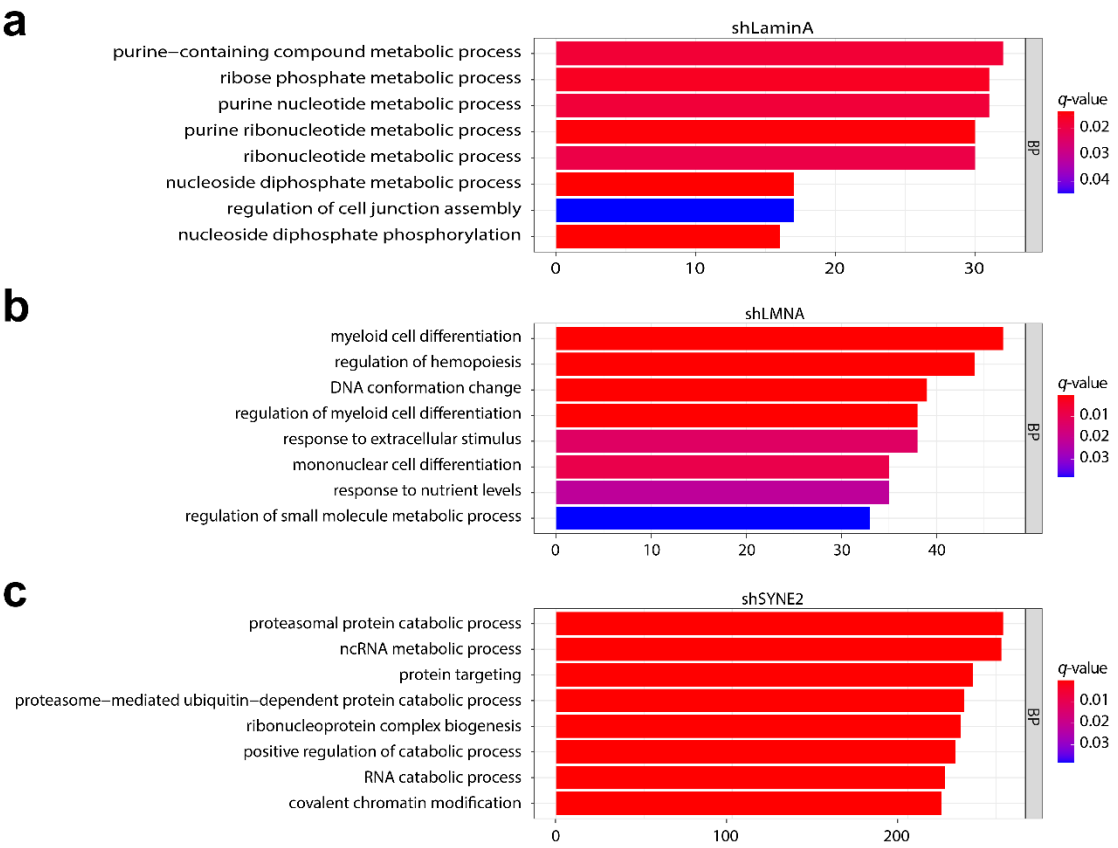

Figure 2. Impact of Lamins and Nesprins on RNA Biosynthesis, Chromatin Conformation, and Modification. DEGs were identified using the DESeq2 package by comparing the doxycycline-treated group to the untreated group. Gene Ontology (GO) enrichment analysis of DEGs was conducted using the clusterProfiler package. The top pathways were selected based on a *q*-value cutoff of < 0.05 for shLaminA (**a**), shLMNA (**b**), and shSYNE2 (**c**), respectively.

Figure 3

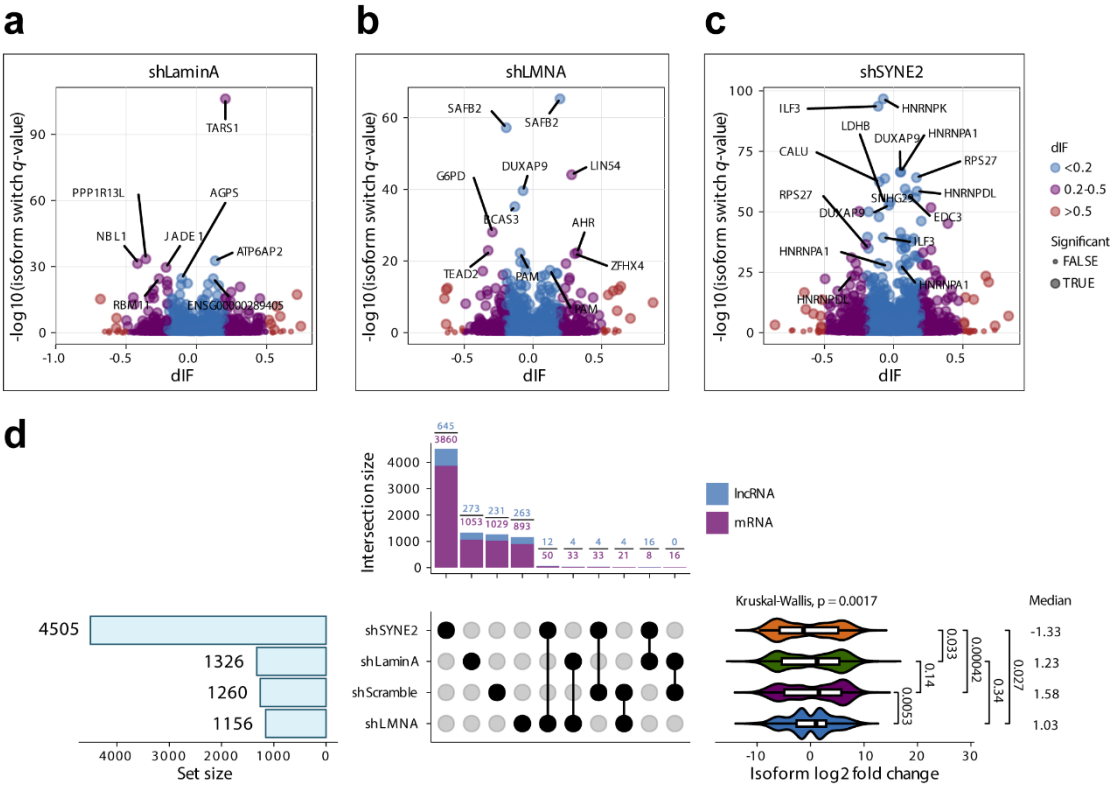

Figure 3. Roles of Lamins and Nesprins in Isoform Switching. a, b, c) Volcano plots illustrating the dIF of differentially expressed isoform transcripts against the -log10 of the isoform switch q-values in shLaminA (a), shLMNA (b), and shSYNE2 (c). Isoform switching was detected using IsoformSwitchAnalyzeR (n = 3 per group, cutoff dIF > 0.1, *q*-value < 0.05). a) Lamin A knockdown leads to isoform switching in chromatin remodeling (JADE1) and alternative splicing regulation (RBM11). b) LMNA knockdown results in isoform switching of transcriptional repressors (SAFB2, LIN54) and transcription factors (TEAD2, AHR). c) SYNE2 knockdown significantly alters isoform ratios of RNA-binding proteins (HNRNPK, ILF3, HNRNPA1). d) UpSet plot displaying the number and overlap of differentially expressed protein-coding mRNAs and lncRNAs, as well as the log2 fold change of isoform

transcripts in shLaminA, shLMNA, and shSYNE2 conditions. Intersection sizes indicate the number of shared DEGs between knockdowns. Statistical analysis was performed using the non-parametric Kruskal-Wallis test to compare medians across multiple groups.

Figure 4

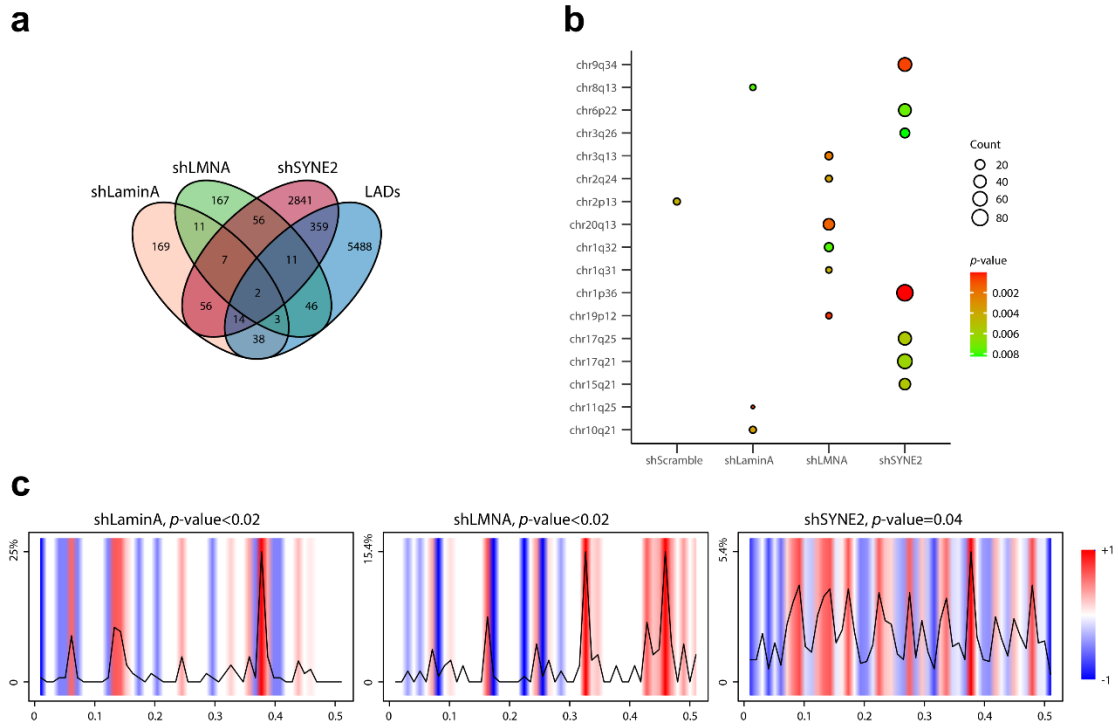

Figure 4. Regulation of gene expression in distal non-LAD regions by lamins and nesprins. a) Venn diagram illustrating the number of DE mRNAs in shLaminA (yellow), shLMNA (green), and shSYNE2 (red), with minimal overlap with genes located in LADs (blue). LAD-associated genes were identified using a BED file derived from Lamin A/C ChIP-seq data[28]. **b)** GO enrichment analysis showing the genomic distribution of DEGs across chromosome arms. for shLaminA, shLMNA, and shSYNE2. The *p*-values (blue to red), and the counts of DE genes mapped to the reference chromosome coordinates are shown. Depletion of Lamin A affects chr10q12, LMNA affects chr20q13, and SYNE2 affects chr9q34, chr1q36. **c)** DE genes from shLaminA, shLMNA, and shSYNE2 are spatially distant from LADs. GenometriCorr analysis quantifying spatial distance between LADs and DEGs. The relative distance from DE genes (query features) to LADs (reference feature) is

plotted by GenometriCorr package (v 1.1.24). the color depicting deviation from the expected distribution and the line indicating the density of the data at relative distance are shown. Statistical analysis performed using Jaccard test, *p*-value < 0.05.

Figure 5

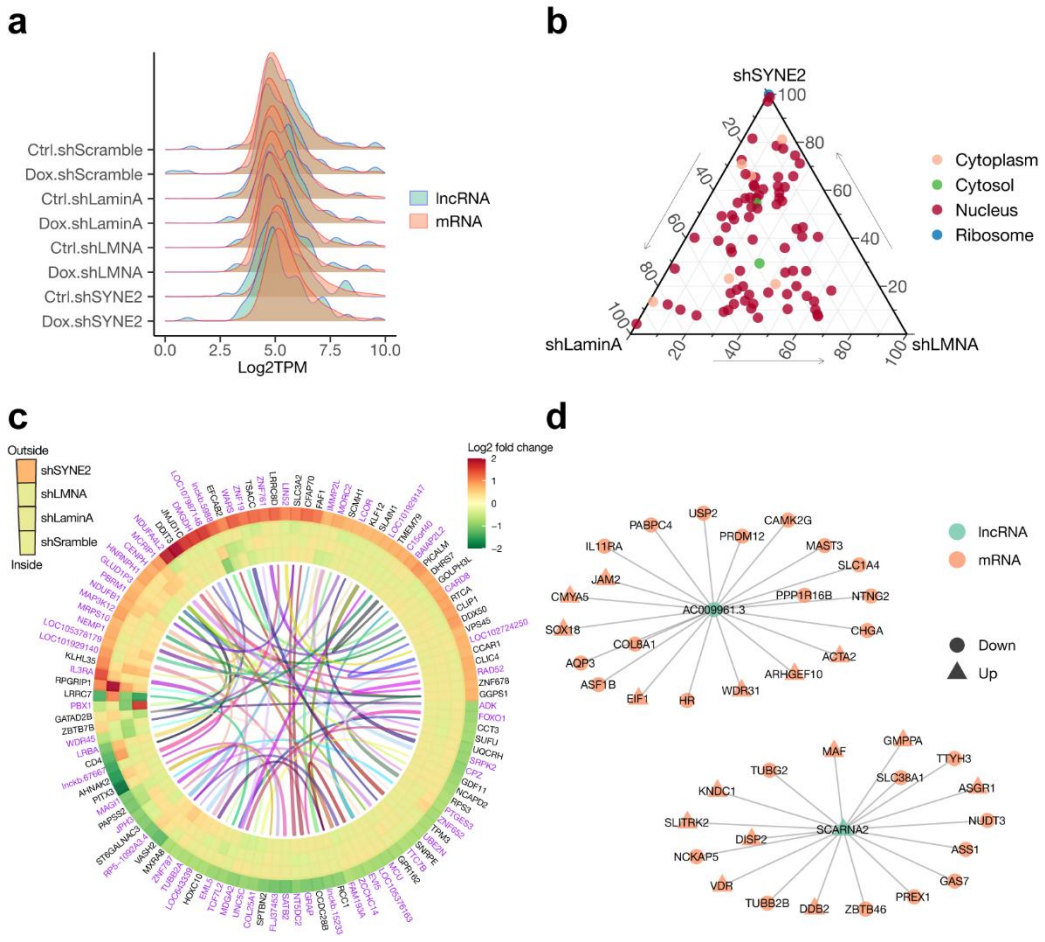

Figure 5. Modulation of lncRNA-mRNA Interactions by Lamins and Nesprins. **a)** Expression distribution of lncRNAs versus mRNAs in log2 transcript per million (Log2TPM), highlighting differences in transcript abundance. **b)** DeepLncLoc predictions showing nuclear localization of identified lncRNAs. **c)** Cis-acting lncRNA-mRNA interaction network predicted based on highly correlated expression levels within 10 kb windows (Pearson correlation > 0.8, *q*-value < 0.05). **d)** Coexpression network analysis of lncRNA-mRNA interactions. Nodes represent transcripts; edges denote coexpression relationships (Pearson correlation > 0.8, *q*-value < 0.05).

598

Figure 6

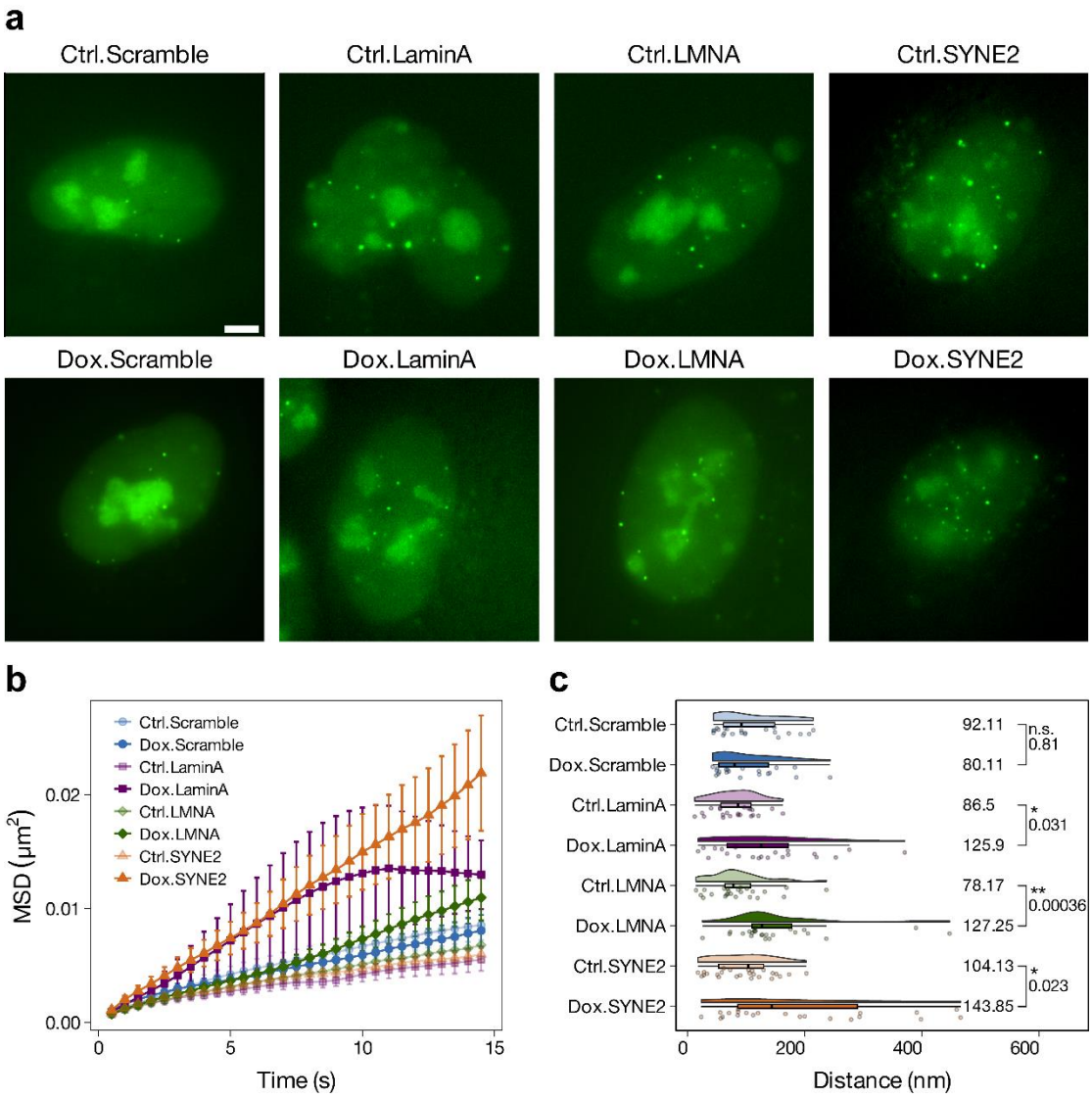

Figure 6. Increased telomere dynamics following depletion of lamin A, LMNA, and SYNE2. a) Representative fluorescence images of telomeres labeled with EGFP-dCas9 in U2OS cells. Cells expressing dCas9-EGFP, targeted to telomeric repeats, were imaged via TIRF microscopy**.** Scale bar = 5 µm. **b)** Mean Square Displacement (MSD) analysis of telomere mobility in control (shScramble) and knockdown conditions (shLaminA, shLMNA, shSYNE2) at 500 ms interval points for 30 s. MSD curves represent n > 20 cells per group. **c)** Total telomere movement range

tracked over a 30 s imaging window. Annotated numbers indicate the median values for each group. Statistical analysis was performed using the non-parametric Kruskal-Wallis test, with a significance threshold of *p-value < 0.05, **p-value < 0.001, and n.s. p-value > 0.05.